Sparsity-Based Ranging for Dual-Frequency Radars

Fauzia Ahmad*, Khodour Al Kadry, and Moeness G. Amin

Radar Imaging Lab, Center for Advanced Communications, Villanova University, Villanova, PA 19085, USA.

ABSTRACT

Dual-frequency radars offer the benefit of reduced complexity, fast computation time, and real-time target tracking in through-the-wall and urban sensing applications. Compared to single-frequency (Doppler) radar, the use of an additional frequency increases the maximum unambiguous range of dual-frequency radars to acceptable values for indoor target range estimation. Conventional dual-frequency technique uses phase comparison of the transmitted and received continuous-wave signals to provide an estimate of the target range. The case of multiple moving targets is handled by separating the different Doppler signatures prior to phase estimation. However, the dual-frequency approach for range estimation can be compromised due to the presence of noise and multipath. In this paper, we investigate a sparsity-based ranging approach as an alternative to the phase difference based technique for dual-frequency radar measurements. Supporting results based on computer simulations are provided that illustrate the advantages of the sparsity-based ranging technique over the conventional method.

Keywords: Dual frequency radar, range-to-motion, compressive sensing, through-the-wall radar.

1. INTRODUCTION

Detection and localization of moving targets are highly desirable in through-the-wall radar sensing applications, such as surveillance and reconnaissance, survivor search in natural disasters, and hostage rescue missions.[1-5] There are several levels of moving target information that could be provided to the radar operator. A zero-dimensional system only provides motion detection capability, while a one-dimensional (1-D) system can provide range-to-motion information. On the other hand, two-dimensional (2-D) and three-dimensional (3-D) systems can localize moving targets in both range and azimuth, with the 3-D system also adding the target elevation information. However, the higher offerings of the 2-D and 3-D systems are obtained at the expense of increased cost, size, weight, and complexity.[6]

In this paper, we consider a 1-D system for localizing moving targets, since a 1-D system provides a good compromise between the level of situational awareness and cost versus size, weight, and complexity. More specifically, we are interested in a low cost, low complexity 1-D system for range-to-motion estimation. Instead of wideband pulsed or stepped-frequency radar systems,[7-9] we employ dual-frequency radars, which estimate the target range by phase comparison of the radar returns at two carrier frequencies.[10,11] The maximum unambiguous range for the dual-frequency approach depends on the frequency difference between the two carrier signals, and, thus, the two frequencies can be chosen to satisfy any desired range ambiguity, e.g., the spatial extent of the urban structure being interrogated. The system requirements of low cost and reduced complexity for through-the-wall operations are met by the dual-frequency radar systems.[12]

A shortcoming of the dual-frequency approach is its inability to estimate the ranges of multiple moving targets, as the phase terms induced by different targets cannot be separated in the time domain. Doppler filtering[5] and time-frequency signal representations[13] have been proposed for separating the different Doppler signatures prior to phase estimation in order to handle multiple moving targets. Note that these preprocessing steps are able to overcome the inherent drawback of the dual-frequency approach provided that the multiple target returns have distinct Doppler signatures.

In this paper, we investigate the offerings of sparsity-based range-to-motion estimation, which is used in lieu of the conventional phase comparison based approach. We consider a sparse scene of either one or two targets moving behind walls. We present the dual-frequency based linear modeling formulation with sensing matrices so as to perform sparse

*fauzia.ahmad@villanova.edu; http://www1.villanova.edu/villanova/engineering/research/centers/cac/facilities/rillab.html

reconstruction of the range-velocity target space. We show that the sparsity based technique suffers from the same limitations as the Doppler preprocessing based dual-frequency approach. However, unlike the conventional approach, it offers the means for simultaneous range-to-motion estimation of multiple moving targets with distinct Doppler signatures. Moreover, we show that the sparse reconstruction based approach provides a higher estimation accuracy compared to the conventional scheme when some of the time samples of the baseband returns at the two frequencies are unavailable due to corruption by noise or interference.

The remainder of the paper is organized as follows. The conventional dual-frequency technique is presented in Section 2. Section 3 describes the dual-frequency based linear model relating the measurements and the unknown target space, and the sparsity-based reconstruction approach. Supporting simulation results are provided in Section 4, followed by concluding remarks in Section 5.

2. DOPPLER PREPROCESSING BASED DUAL-FREQUENCY APPROACH

Consider a dual-frequency Doppler radar employing two known carrier frequencies, f_1 and f_2, and a scene of K moving targets. The kth target is assumed to be undergoing uniform motion with a constant velocity v_k, with its corresponding range expressed as

$$R_k(t) = R_{0k} + v_k \cos(\theta_k)t, \quad k = 1,2,\ldots,K \tag{1}$$

Here, R_{0k} is the initial range to the kth target at time $t = 0$ and θ_k is the aspect angle of the kth target with respect to the radar line-of-sight. Without loss of generality, θ_k is assumed to be zero for all k. The baseband radar returns corresponding to the K moving targets at each frequency can be expressed as,

$$\begin{aligned} s_i(t) &= \sum_{k=1}^{K} \rho_k \exp\left(-j\frac{4\pi f_i R_k(t)}{c}\right), \quad i = 1,2 \\ &= \sum_{k=1}^{K} \rho_k \exp\left(-j\frac{4\pi f_i R_{0k}}{c}\right).\exp\left(-j\frac{4\pi v_k f_i t}{c}\right), \end{aligned} \tag{2}$$

where c is the speed of light and ρ_k is the amplitude of the kth target return, which is taken to be identical for the two frequencies since the difference in the carrier frequencies is assumed small. The Doppler frequency shifts are differentials of the corresponding phases and are given by,

$$\tilde{f}_{ik} = \frac{2v_k f_i}{c}, i = 1,2, \quad k = 1,2,\ldots,K. \tag{3}$$

Then, (2) can be rewritten as

$$s_i(t) = \sum_{k=1}^{K} \rho_k \exp\left(-j\frac{4\pi f_i R_{0k}}{c}\right)\exp\left(-j2\pi\tilde{f}_{ik}t\right), \quad i = 1,2. \tag{4}$$

Taking the Fourier transform of $s_i(t)$, we obtain

$$S_i(f) = \sum_{k=1}^{K} \rho_k \exp\left(-j\frac{4\pi f_i R_{0k}}{c}\right)\delta(f - \tilde{f}_{ik}), \quad i = 1,2 \tag{5}$$

where $\delta(\cdot)$ is the Dirac delta function. Thus, the Doppler spectrum corresponding to the ith frequency exhibits peaks at the Doppler shifts associated with the K targets. The associated phases in (5) corresponding to the two operational frequencies can be extracted for each target separately in the Doppler domain as

$$\phi_{ik} = \frac{4\pi f_i R_{0k}}{c}, \; i = 1,2, \quad k = 1,2,\ldots,K. \tag{6}$$

Accordingly, the initial range of each target can be obtained by phase comparison as

$$R_{0k} = \frac{c}{4\pi(f_2 - f_1)}(\phi_{2k} - \phi_{1k}), \quad i = 1, 2, \quad k = 1,2,\ldots, K, \tag{7}$$

whereas the target velocities can be directly obtained from the Doppler shifts. Note that this scheme works as long as the K targets are moving with distinct velocities.

3. SPARSITY-BASED RANGE AND VELOCITY ESTIMATION

3.1 Linear Signal Model and Sparse Reconstruction

We sample the baseband returns $s_i(t)$ at times $\{t_n\}_{n=0}^{N-1}$ and append the N time samples at each of the two carrier frequencies, f_1 and f_2, to form a tall measurement vector as

$$\boldsymbol{s} = \begin{bmatrix} s_1(0) & s_1(1) & \ldots & s_1(N-1) & s_2(0) & s_2(1) & \ldots & s_2(N-1) \end{bmatrix}^T. \tag{8}$$

Assume that the target space is divided into $M \times L$ grid-points in range and velocity. We form the concatenated $ML \times 1$ weighted target indicator vector $\boldsymbol{r}$ corresponding to the range-velocity sampling grid, i.e., if there is a target present at the mth range bin and lth velocity bin, then the corresponding element of $\boldsymbol{r}$ should be non-zero; otherwise, it is zero. Then, using the model in (2), we obtain the linear system of equations

$$\boldsymbol{s} = [\boldsymbol{\Psi}_1^T \quad \boldsymbol{\Psi}_2^T]^T \boldsymbol{r} = \boldsymbol{\Psi} \boldsymbol{r} \tag{9}$$

where $\boldsymbol{\Psi}$ is the $2N \times ML$ dictionary matrix and the nth row of the $N \times ML$ matrix $\boldsymbol{\Psi}_i$ is given by

$$[\boldsymbol{\Psi}_i]_n = \left[\exp\left(-j \frac{4\pi(R_0 + v_0 n)}{c} f_i \right) \quad \exp\left(-j \frac{4\pi(R_1 + v_0 n)}{c} f_i \right) \quad \cdots \quad \exp\left(-j \frac{4\pi(R_{M-1} + v_{L-1} n)}{c} f_i \right) \right]. \tag{10}$$

In other words, for a scene with K moving targets, the measurement vector $\boldsymbol{s}$ is a linear combination of only K specific columns from the dictionary $\boldsymbol{\Psi}$. In order to recover the target indicator vector, we need to determine which columns of $\boldsymbol{\Psi}$ contribute to the measurement vector $\boldsymbol{s}$. This can be accomplished through use of greedy sparse approximation methods,[14] which determine the support of the sparse vector in an iterative manner. In this paper, we use orthogonal matching pursuit (OMP) for the sparsity based reconstruction.[15]

3.2 Sparse Reconstruction of a Single Moving Target

For a single moving target with initial range R_{01} and velocity v_1, a single iteration of the OMP algorithm is required to recover the target indicator vector. The column index of $\boldsymbol{\Psi}$ that corresponds to the target range-velocity grid-point is identified by locating the position of the highest peak of the $ML \times 1$ vector $\boldsymbol{y} = \boldsymbol{\Psi}^H \boldsymbol{s}$. Using (5) and (10), the element of $\boldsymbol{y}$ corresponding to the (m, l)th range-velocity grid-point can be expressed as

$$y(R_m, v_l) = \sum_{i=1}^{2} \sum_{n=0}^{N-1} \rho_1 \exp\left(j \frac{4\pi f_i (R_m - R_{01})}{c} \right) \exp\left(j \frac{4\pi (v_l - v_1) f_i n}{c} \right). \tag{11}$$

It is clear from (11) that the highest peak of $\boldsymbol{y}$ occurs when $R_m = R_{01}$ and $v_l = v_1$, thereby correctly identifying the support of the target indicator vector $\boldsymbol{r}$. The estimate $\hat{\boldsymbol{r}}$ is obtained as $\hat{\boldsymbol{r}} = \boldsymbol{\psi}^{\dagger} \boldsymbol{s}$, where $\boldsymbol{\psi}^{\dagger}$ is the pseudoinverse of the column of $\boldsymbol{\Psi}$ corresponding to the identified index.

3.3 Sparse Reconstruction of Two Moving Targets

Similar to the sparse reconstruction of a single moving target, it can be shown in a straightforward manner that two iterations of the OMP algorithm identify the correct set of column indices of $\boldsymbol{\Psi}$ for the case of two targets moving with different velocities.

Next, we consider two targets of equal amplitudes ($\rho_1 = \rho_2 = \rho$) at initial ranges R_{01} and R_{02}, both moving with the same velocity v. Two OMP iterations are required to localize the two targets. The first iteration of OMP will locate the index that corresponds to the highest peak position of $\boldsymbol{y} = \boldsymbol{\Psi}^H \boldsymbol{s}$. In this case, the element of $\boldsymbol{y}$ corresponding to the (m, l)th range-velocity grid-point can be expressed as

$$y(R_m, v_l) = \sum_{i=1}^{2} \sum_{n=0}^{N-1} \rho \left[\exp\left(j \frac{4\pi f_i (R_m - R_{01})}{c} \right) + \exp\left(j \frac{4\pi f_i (R_m - R_{02})}{c} \right) \right] \exp\left(j \frac{4\pi (v_l - v) f_i n}{c} \right). \tag{12}$$

Eq. (12) can be simplified as

$$y(R_m, v_l) = \sum_{i=1}^{2} \sum_{n=0}^{N-1} \rho \sqrt{2\left(1 + \cos\left(\frac{4\pi f_i (R_{02} - R_{01})}{c} \right)\right)} \exp\left(j \frac{4\pi f_i}{c} \left(R_m - \frac{R_{02} + R_{01}}{2} \right) \right) \exp\left(j \frac{4\pi (v_l - v) f_i n}{c} \right). \tag{13}$$

which implies that the highest peak will occur for the grid-point corresponding to $R_m = \dfrac{R_{02} + R_{01}}{2}$ and $v_l = v$. That is, the first iteration fails to identify a valid target initial range. As a result, the subsequent iteration will also produce an erroneous index value. Thus, similar to conventional dual-frequency algorithm, the sparsity based scheme will fail to localize two targets moving with the same velocity.

3.4 Sparse Reconstruction under Reduced Time Samples

The signal model in (9) can be extended to the case where some of the time samples at each frequency are unavailable due to intentional or unintentional interference and/or impulsive noise. This is accomplished through the introduction of an $N_A \times 2N$ ($N_A < 2N$) measurement matrix $\boldsymbol{\Phi}$ to obtain the reduced set of measurements as

$$\bar{\boldsymbol{s}} = \boldsymbol{\Phi} \boldsymbol{\Psi} \boldsymbol{r} \tag{14}$$

The measurement matrix can be of different types, as reported in Refs. [16-18]. Given the reduced measurement vector $\bar{\boldsymbol{s}}$ of length N_A, we can recover $\boldsymbol{r}$ in a manner similar to that for the full measurement set case. Again, the sparsity based scheme will work as long as the multiple targets are moving with different velocities and a sufficient number of samples are available. More details on the relation between the number of samples and the scene sparsity for OMP can be found in Ref. [15].

4. SIMULATION RESULTS

We present simulation results for localization of point targets undergoing uniform motion using the sparse reconstruction scheme under both cases of full and partial availability of time samples at the two carrier frequencies. Conventional Doppler preprocessing based dual-frequency results are also provided in each case for comparison. The carrier frequencies used in the simulation are $f_1 = 990$ MHz and $f_1 = 1$ GHz, yielding an unambiguous range of 15 m. The target space extends from 0 to 15 m in range and -1 m/s to +1 m/s in velocity and is divided into 15×21 grid points in range and velocity, resulting in 315 unknowns. The time response of the target space at each carrier frequency consists of $N = 100$ time samples. Independent and identically distributed Gaussian noise with a signal-to-noise ratio (SNR) of 0 dB is added to the measurements at each carrier frequency.

Three different configurations of two unit-amplitude moving targets ($\rho_1 = \rho_2 = 1$) are considered. First, the two targets are assumed to be at initial ranges $R_{01} = 3$ m and $R_{02} = 6$ m, moving with respective velocities $v_1 = -0.3$ m/s and $v_2 = 0.5$ m/s. Fig. 1 shows the joint range-velocity estimates of the two moving target scene obtained with OMP using all $2N = 200$ time samples. We can clearly see that the sparse reconstruction approach provides accurate range and velocity estimates of both targets. For comparison, the conventional approach is also used to estimate the target ranges and velocities. Fig. 2 depicts the Doppler spectra corresponding to the two carrier frequencies. The true target Doppler shifts are indicated by red dashed lines. We observe that the peaks coincide in each case with the correct Doppler frequencies. The initial range estimates, obtained using the phases extracted from the Doppler domain in (7), are 3.30 m, and 6.19 m, respectively. The biases in the conventional range estimates are attributed to the low SNR.[19]

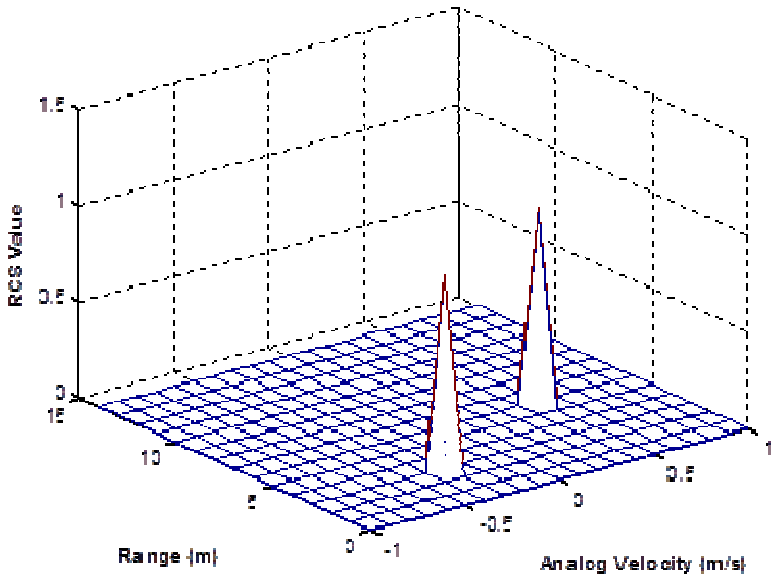

Figure 1. Sparse reconstruction result for two moving targets initially at 3 m and 6 m, moving with -0.3m/s and 0.5 m/s, respectively.

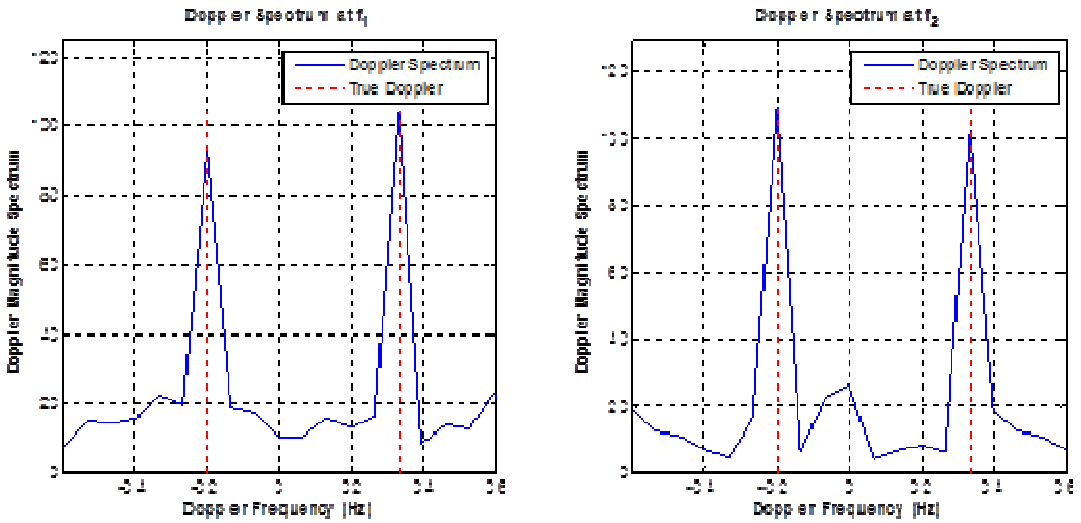

(a) (b)

Figure 2. Doppler Spectrum of two targets initially at 3 m and 6 m, moving with -0.3 m/s and 0.5 m/s at (a) the first carrier frequency and (b) the second carrier frequency.

Next, we consider two point targets at the same initial range, i.e., $R_{01} = R_{02} = 6$ m, and moving with respective velocities $v_1 = -0.3$ m/s and $v_2 = 0.5$ m/s. Fig. 3 shows the corresponding range-velocity estimates obtained with OMP using all $2N = 200$ time samples. The sparse reconstruction approach provides accurate range and velocity estimates of both targets in this case as well. On the other hand, the conventional approach provides biased initial range estimates of 6.04 m and 5.98 m, which are obtained using the phases extracted from the Doppler spectra corresponding to the two carrier frequencies shown in Fig. 4.

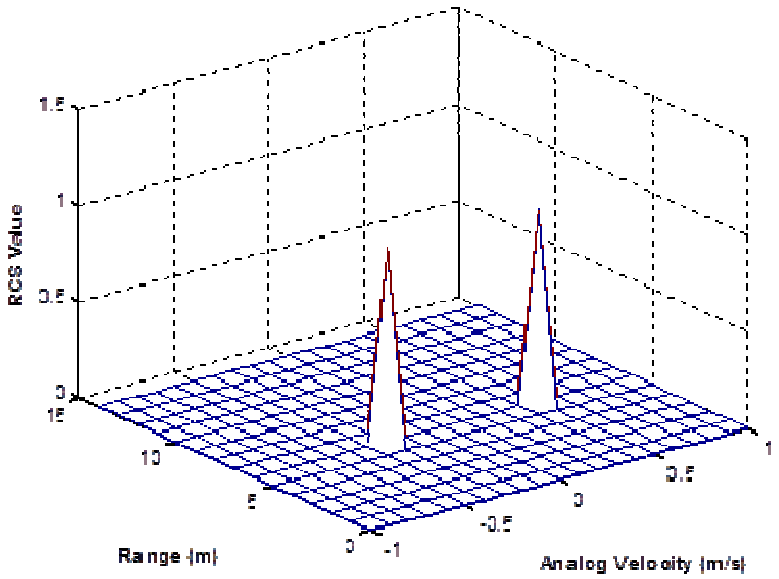

Figure 3. Sparse reconstruction result for two targets both initially at 6 m, moving with -0.3 m/s and 0.5 m/s, respectively.

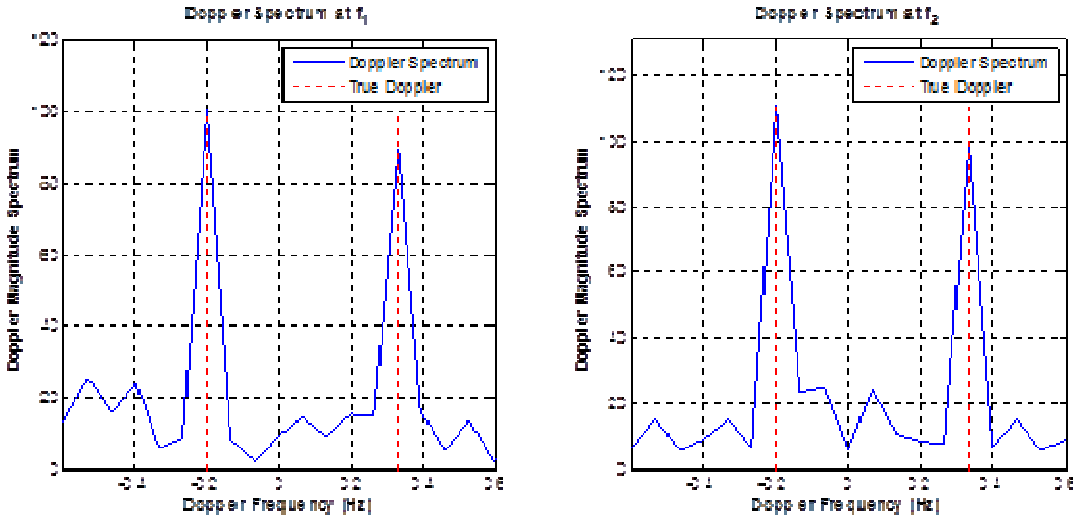

(a) (b)

Figure 4. Doppler Spectrum of two targets both initially at 6 m, moving with -0.3 m/s and 0.5 m/s at (a) the first carrier frequency and (b) the second carrier frequency.

The third case assumes two point targets at initial ranges $R_{01} = 4$ m and $R_{02} = 6$ m, both moving with the same velocity $v_1 = v_2 = 0.5$ m/s. Fig. 5 depicts the sparse reconstruction result obtained with OMP using all $2N = 200$ time samples. As expected, the sparsity-based approach fails to correctly localize the two targets in the range-Doppler space. The Doppler filtering approach fails as well because the target returns cannot be separated in the Doppler domain as shown in Fig. 6.

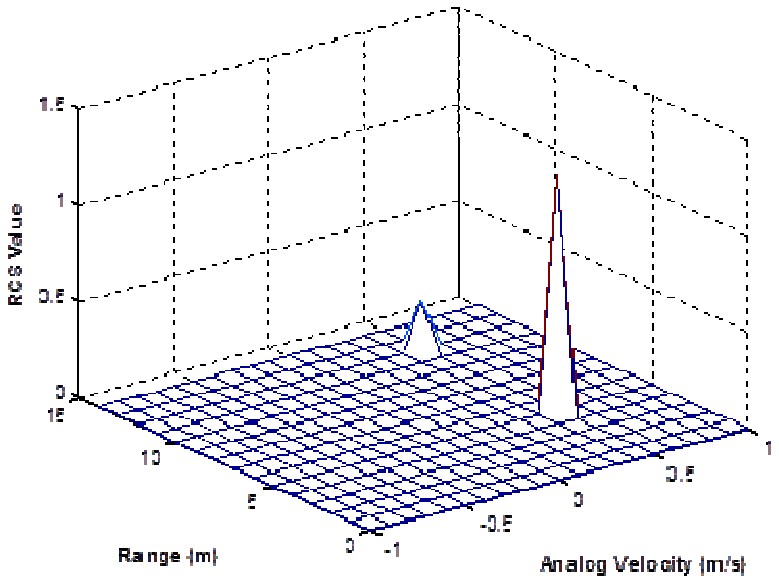

Figure 5. Sparse reconstruction result for two targets initially at 4 m and 6 m, both moving at 0.5m/s

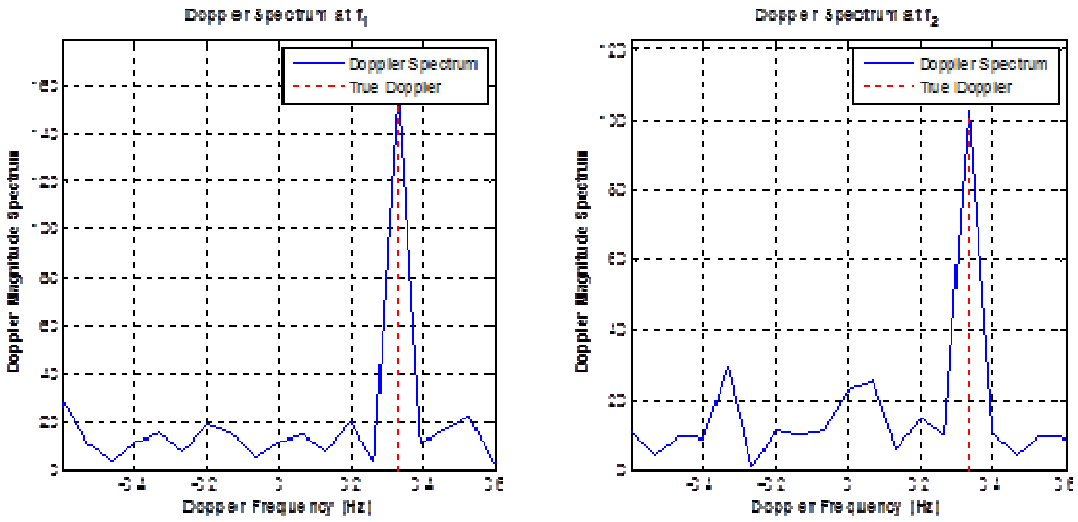

(a) (b)

Figure 6. Doppler Spectrum of two targets initially at 4 m and 6 m, both moving with 0.5 m/s at (a) the first carrier frequency and (b) the second carrier frequency.

Finally, we consider the case of limited availability of the time samples at the two carrier frequencies. We assume that only 5 randomly selected samples are available at each carrier frequency, leading to $N_A = 10$. The two targets are assumed to be initially at $R_{01} = 3$ m and $R_{02} = 6$ m, moving with respective velocities $v_1 = -0.3$ m/s and $v_2 = 0.5$ m/s. Fig. 7 shows the sparse reconstruction result, which clearly yields accurate estimates of the range-velocity pairs associated with the two targets. Fig. 8 shows the Doppler spectra at the two carrier frequencies using the limited time samples (the unavailable samples were taken as zero in the Fourier transform operation). Clearly, the high aliasing noise power due to the randomized 5% time samples overwhelms the signal Doppler spectra,[20] and renders target localization infeasible.

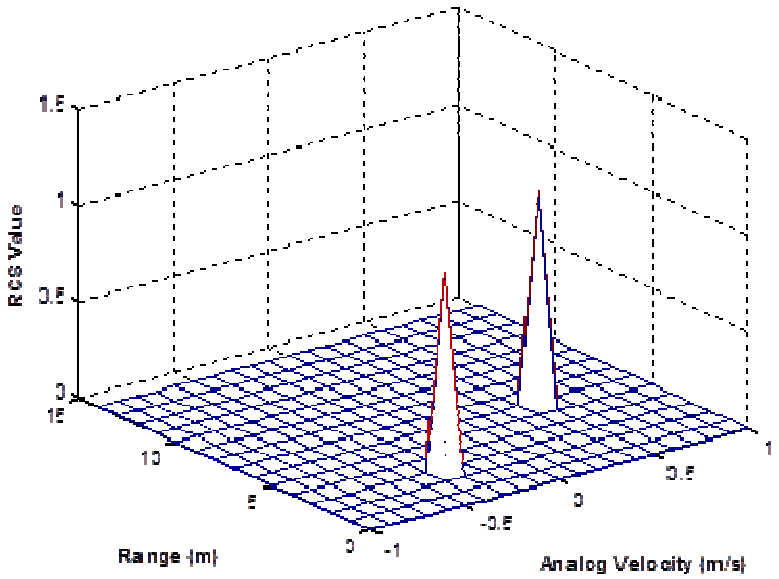

Figure 7. Sparse reconstruction result using 5% of the measurements for the case of two moving targets initially at 3 m and 6 m, moving with velocities -0.3 m/s and 0.5 m/s.

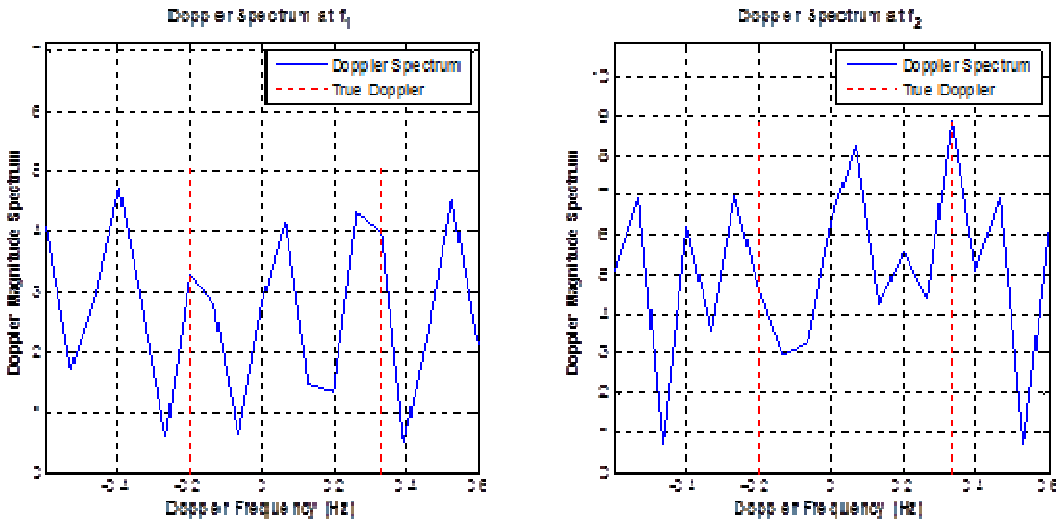

Figure 8. Doppler Spectrum of two targets initially at 3 m and 6 m, moving with -0.3 m/s and 0.5 m/s using 5% of measurements at (a) the first carrier frequency and (b) the second carrier frequency.

5. CONCLUSION

In this paper, we presented a moving target localization approach based on sparse reconstruction for dual-frequency radar measurements. Unlike the two-step conventional dual-frequency approach that requires Doppler preprocessing followed by phase comparison for target localization, the sparsity-based technique can jointly estimate the range and velocity of the moving targets. Moreover, it is able to accurately localize the targets in range-velocity space even when some of the time samples are corrupted by noise or interference and are thus unavailable. However, similar to the conventional approach, the sparsity based scheme can localize moving targets only when they are moving with distinct velocities. Supporting results based on computer simulation are provided under both full and partial availability of time samples at the two carrier frequencies.

ACKNOWLEDGMENT

This work was supported by ARO and ARL under contract W911NF-11-1-0536.

REFERENCES

[1] Amin, M.G. (Ed.), [Through-the-Wall Radar Imaging], CRC Press, Boca Raton, FL (2011).
[2] Hong Wang, Narayanan, R.M., and Zhengou Zhou, "Through-Wall Imaging of Moving Targets using UWB Random Noise Radar," IEEE Antennas Wireless Propag. Lett 8, 802-805 (2009).
[3] Ahmad, F., Amin, M.G. and Setlur, P., "Through-the-Wall Target Localization using Dual-Frequency CW Radars," Proc. SPIE. 6201, 62010H (2006).
[4] Amin, M., Zemany, P., Setlur, P. and Ahmad, F., "Moving Target Localization for Indoor Imaging using Dual Frequency CW Radars," Proc. Fourth IEEE Workshop on Sensor Array and Multi-Channel Process., 367-371 (2006).
[5] Lin, A. and Ling, H., "Location tracking of indoor movers using a two-frequency Doppler and direction-of-arrival (DDOA) radar," Digest IEEE Int. Symp. Antennas Propag., 1125 – 1128 (2006).
[6] Amin, M. (Ed.), Special Issue on 'Advances in Indoor Radar Imaging,' J. Franklin Institute 345(6), 556-722 (2008).
[7] Ranney, K., et al., "Recent MTI experiments using ARL's synchronous impulse reconstruction (SIRE) radar," Proc. SPIE 6947, 694708 (2008).
[8] Maaref, N., et al., "A study of UWB FM-CW radar for the detection of human beings in motion inside a building," IEEE Trans. Geosci. Remote Sens. 47(5), 1297-1300 (2009).
[9] Amin, M.G. and Ahmad, F., "Change Detection Analysis of Humans Moving Behind Walls," IEEE Trans. Aerosp. Electronic Syst. 49(3), 1410-1425 (2013).
[10] Ridenour, L.N., [Radar System Engineering, vol. 1 of MIT Radiation Laboratory Series], McGraw-Hill, NY (1947).
[11] Boyer, W.D., "A diplex, Doppler, phase comparison radar," IEEE Trans. Aerosp. Navig. Electron. ANE-10(3), 27-33 (1963).
[12] Ahmad, F., Amin, M.G. and Zemany, P.D., "Dual-Frequency Radars for Target Localization in Urban Sensing," IEEE Trans. Aerosp. Electronic Syst. 45(4), 1598-1609 (2009).
[13] Zhang, Y., Amin, M. G. and Ahmad, F., "A Novel Approach for Multiple Moving Target Localization using Dual-Frequency Radars and Time-Frequency Distributions," Proc. 41th Annual Asilomar Conf. Signals, Systems, and Computers, 1817-1821 (2007).
[14] Tropp, J.A., "Greed is good: Algorithmic results for sparse approximation," IEEE Trans. Inf. Theory 50(10), 2231–2242 (2004).
[15] Tropp, J.A. and Gilbert, A.C., "Signal recovery from random measurements via orthogonal matching pursuit," IEEE Trans. Inf. Theory 53(12), 4655–4666 (2007).
[16] Gurbuz, A., McClellan, J., and Scott Jr., W., "Compressive sensing for subsurface imaging using ground penetrating radar, " Signal Process. 89(10), 1959-1972 (2009).
[17] Potter, L.C., Ertin, E., Parker, J. T. and Cetin, M., "Sparsity and compressed sensing in radar imaging," Proc. of the IEEE 98(6), 1006-1020 (2010).
[18] Qian, J., Ahmad, F., and Amin, M.G., "Joint localization of stationary and moving targets behind walls using sparse scene recovery," J. Electronic Imag. 22(2), 021002 (2013).
[19] Ahmad, F., Amin, M. G. and Zemany, P.D., "Performance analysis of dual-frequency CW radars for motion detection and ranging in urban sensing applications," Proc. SPIE 6547, 65470K (2007).
[20] Luo, C. and McClellan, J.H.,"Discrete Random Sampling Theory", Proc. IEEE Int. Conf. Acoustics, Speech and Signal Process., 5430-5434 (2013).